

13. SITE 564¹

Shipboard Scientific Party²

HOLE 564

Date occupied: 28 October 1981

Date departed: 1 November 1981

Time on hole: 96 hr.

Position (latitude; longitude): 33°44.36'N; 43°46.03'W

Water depth (sea level; corrected m, echo-sounding): 3820

Water depth (rig floor; corrected m, echo-sounding): 3830

Bottom felt (m, drill pipe): 3830

Penetration (m): 365

Number of cores: 9

Total length of cored section (m): 81

Total core recovered (m): 34.75

Core recovery (%): 43

Oldest sediment cored:

Depth sub-bottom (m): 284+ (in the basement)

Nature: Limestone

Age: lower Oligocene

Basement:

Depth sub-bottom (m): 284

Nature: Basalt

Principal results: Hole 564 (Site MAR-11) was drilled on Anomaly 13 on the west flank of the Mid-Atlantic Ridge about 60 miles south of the Hayes Fracture Zone (Fig. 1). Site 564 is located about 6 miles north of Site 563.

The sediments were washed down to the basement, which was felt at a depth of 284 m sub-bottom. The basement was cored for 81 m. It is composed of aphyric basalts (both pillows and massive units) belonging to a single petrographic chemical group, even though some small variations close to the limit of precision of concentration measurements are observed. Nb varies from 2.8 to 6.1, Zr from 86 to 100, Ti from 8250 to 9000, Y from 38 to 42, and V

from 345 to 463 (all measured in ppm). This range of variation is consistent with either depleted ($[Nb/Zr]_{ch} \sim 0.38$) or flat ($[Nb/Zr]_{ch} \sim 0.54$) rare earth patterns, but additional onshore measurements are needed to confirm this downhole variation.

A complete set of logs was run. As at Sites 556 and 558, two distinct sedimentary units are evident. Two temperature profiles were recorded; the first was run 18 hr. after circulation was stopped and the second 10 hr. later. The two profiles were identical down to below the sediment basement interface, showing a low gradient of about 6°C/km. Between 45 and 60 m in the basement, an increase of 2.5°C was observed. This is additional evidence at Anomaly 13 of downflow of seawater when the sedimentary layer is pierced.

No sediment accumulation rates could be calculated at this site, and no samples were taken for pore-water analysis.

OPERATIONS

Approach to Site

After drilling at Hole 563 ended, we decided to drill a second hole at MAR-11 but located about 5 or 10 miles away from Site 563. The *Challenger* got under way at 0730Z, 28 October, and headed in a northwesterly direction. Within two miles, basement became buried by a thick blanket of sediments. By 0850Z it was apparent that a suitable drill site might not be crossed for a long distance along this track. The course of the *Challenger* was altered to 090°, on a track that would pass about 6 miles north of Site 563 and that might cross the same basement ridge (Fig. 2, site chapter, Site 563, this volume). Upon crossing the ridge, we noted a location at 1005Z that fulfilled the requirements of thin sediments (less than 350 m) and smooth basement (Fig. 2). The course of the *Challenger* was reversed at 1022Z, and the beacon was dropped on Site 564 at 1047Z.

On-Site Operations

Hole 564 was spudded in at 1743Z, 28 October. Sediments were washed to a depth of 284 m sub-bottom where basement was hit. Coring within basement proceeded at a much faster rate than at Site 563 and without any major difficulties. Between 0305Z, 29 October and 1520Z, 30 October, nine cores were recovered, a total basement penetration of 81 m (Table 1). After Core 9 was recovered and we found out that a tropical storm might pass close by within 24 hr., we decided to begin logging operations three hours earlier than originally planned. The logging operations, which are described in detail in the Downhole Measurements section, proceeded smoothly and the tropical storm did not appear. Logging was completed at 2355Z, 31 October, and the drill string was pulled for the final time on Leg 82. The *Challenger* started on course to the Virgin Islands at 0847Z, 1 November.

¹ Bougault, H., Cande, S. C., et al., *Init. Repts. DSDP*, 82: Washington (U.S. Govt. Printing Office).

² Henri Bougault (Co-Chief Scientist), IFREMER (formerly CNEXO), Centre de Brest, B. P. 337, 29273 Brest Cedex, France; Steven C. Cande (Co-Chief Scientist), Lamont-Doherty Geological Observatory, Columbia University, Palisades, New York; Joyce Brannon, Department of Earth and Planetary Sciences, Washington University, St. Louis, Missouri; David M. Christie, Hawaii Institute of Geophysics, University of Hawaii at Manoa, Honolulu, Hawaii; Murlene Clark, Department of Geology, Florida State University, Tallahassee, Florida; Doris M. Curtis, Curtis and Echols, Geological Consultants, Houston, Texas; Natalie Drake, Department of Geology, University of Massachusetts, Amherst, Massachusetts; Dorothy Echols, Department of Earth and Planetary Sciences, Washington University, St. Louis, Missouri (present address: Curtis and Echols, Geological Consultants, 800 Anderson, Houston, Texas 77401); Ian Ashley Hill, Department of Geology, University of Leicester, Leicester LE1 7RH, United Kingdom; M. Javed Khan, Lamont-Doherty Geological Observatory, Columbia University, Palisades, New York (present address: Department of Geology, Peshawar University, Peshawar, Pakistan); William Mills, Deep Sea Drilling Project, Scripps Institution of Oceanography, La Jolla, California (present address: Ocean Drilling Program, Texas A&M University, College Station, Texas 77843); Rolf Neuser, Institut für Geologie, Ruhr Universität Bochum, 4630 Bochum 1, Federal Republic of Germany; Marion Rideout, Graduate School of Oceanography, University of Rhode Island, Kingston, Rhode Island (present address: Department of Geology, Rice University, P.O. Box 1892, Houston, Texas 77251); and Barry L. Weaver, Department of Geology, University of Leicester, Leicester, LE1 7RH, United Kingdom (present address: School of Geology and Geophysics, University of Oklahoma, Norman, Oklahoma 73019).

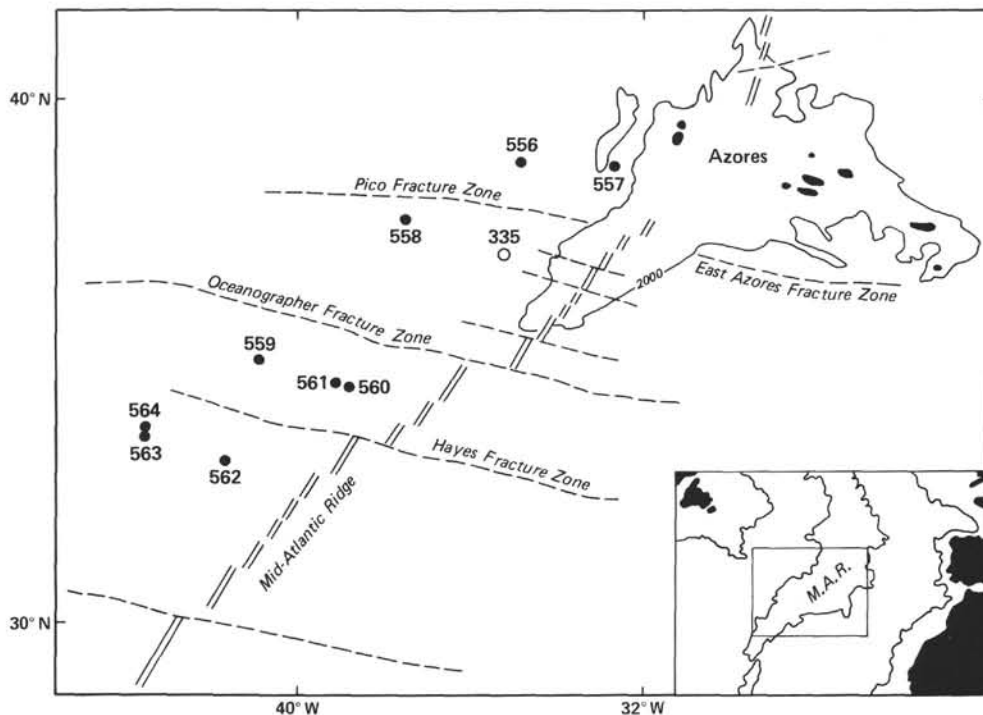


Figure 1. Site location map, Leg 82.

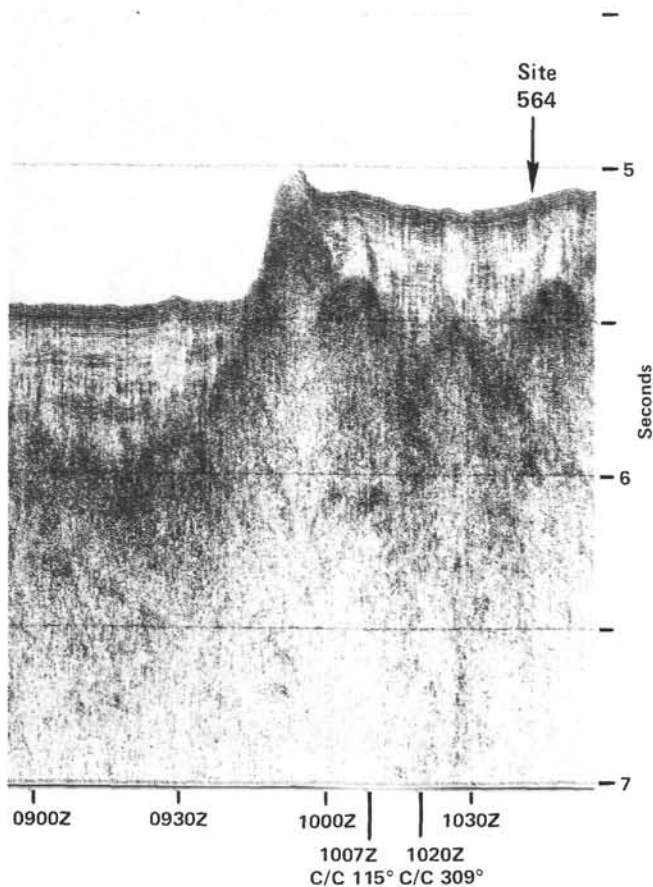


Figure 2. *Glomar Challenger* seismic records of the approach to Site 564. For location of profile see Figure 2, site chapter, Site 563, this volume. C/C = course change.

Table 1. Coring summary, Hole 564.

Core	Date (Oct. 1981)	Time (Z)	Depth from drill floor (m)	Depth below seafloor (m)	Length cored (m)	Length recovered (m)	Percent recovered
H1	28	2122	3830.0-4114.0	0.0-284.0	0.0	0.00	0
1	29	0305	4114.0-4123.0	284.0-293.0	9.0	3.40	38
2	29	0805	4123.0-4132.0	293.0-302.0	9.0	3.44	38
3	29	1240	4132.0-4141.0	302.0-311.0	9.0	4.10	46
4	29	1735	4141.0-4150.0	311.0-320.0	9.0	4.87	54
5	29	2202	4150.0-4159.0	320.0-329.0	9.0	5.19	58
6	30	0312	4159.0-4168.0	329.0-338.0	9.0	5.72	64
7	30	0740	4168.0-4177.0	338.0-347.0	9.0	3.31	37
8	30	1049	4177.0-4186.0	347.0-356.0	9.0	1.98	22
9	30	1520	4186.0-4195.0	356.0-365.0	9.0	2.74	30
					81.0	34.75	43

SEDIMENT LITHOLOGY

At Site 564 a single bit hole was drilled and washed down to basement at 284 m, and 9.6 m (564-H1-1 to 564-H1-7 and 564-H1,CC) of sediment were recovered. The site is located approximately 10 km north of Site 563 on Anomaly 13, in water depth of 3830 m. Although the sediment directly overlying the basalt was not recovered, the core catcher was dated as early Oligocene (34-34.5 Ma).

The 9.6 m of sediment recovered in Core H1 are predominantly foraminiferal nannofossil ooze, with chalky intervals increasing from Section 564-H1-4 downward, and an interval of clayey ooze in Sections 564-H1-3 and 564-H1-4. Section 564-H1-7 and 564-H1,CC contain dolomitic nannofossil chalk and ooze. The sediment colors change from predominantly white and light gray (10YR 8/1-8/2, 5YR 8/1-7/1, 7/2) in Sections 564-H1-1 and 564-H1-2 to brown and yellowish brown (10YR 6/3, 6/4, 5/4, 4/4) in Sections 564-H1-3 to 564-H1-7. Bedding is massive; bioturbation/mottling and burrows are pres-

ent throughout, increasing from mild in Sections 564-H1-1 to 564-H1-3 to moderate in Sections 564-H1-4 and 564-H1-5, but almost absent in Sections 564-H1-6 and 564-H1-7. Carbonate content, measured by carbonate bomb, is over 90% (up to 98%) in all sections except in 564-H1-3 and 564-H1-4 (83–89%). This repeats the results at Site 563. Principal sediment components are nanofossils (60–90%, except for 47% in the dolomitic chalk) and foraminifers (3–25%). Clay content is equal to or less than 10%. Dolomite rhombs are present in Sections 564-H1-6 and 564-H1-7 (2–10%) and 564-H1,CC (15%). Micronodules are present in trace amounts in most samples and are estimated at 3–5% in 564-H1-4 and 564-H1,CC.

We have given this detailed description of the lithologies found in the wash core because it shows the strong similarities to the lithologies at Site 563. Although condensed by discontinuous recovery in wash Core H1, Site 564 contains the same two sediment units with similar lithologic characteristics and similar stratigraphy. Even the transition zone between the units can be recognized in Sections 564-H1-3 and 564-H1-4 where the color changes, the carbonate content decreases slightly, and the samples contain lower middle Miocene to upper lower Miocene nanofossil zones.

BIOSTRATIGRAPHY

Summary

One washed core was retrieved above basement at Site 564. The sediment recovered ranges from lower Oligocene to upper middle Miocene based on calcareous nanofossils. Planktonic foraminifers from 564-H1,CC indicate that the base of the section is Oligocene and belongs to the *Chiloguembelina* Zone (lower NP21).

Calcareous Nanofossils

One washed core (H1) was obtained above basement in Hole 564. The top of 564-H1-1 is upper middle to lower upper Miocene and on the basis of *Discoaster hamatus* is placed in the *D. hamatus* Zone CN7 (NN9). Section 564-H1-7 is assigned to the lower Oligocene *S. predistentus* Zone on the basis of the absence of *S. ciproensis* and *S. distentus*. The core catcher of Core H1 contains *Reticulofenestra umbilica* without *Coccolithus formosus* and belongs to the *Helicosphaera reticulata* Zone, *Reticulofenestra hillae* Subzone CN16c (NP22), which is lower Oligocene.

Both 564-H1-7 and 564-H1,CC contain *Braarudosphaera rosa*. This species is also found in the same stratigraphic range at Site 563 and may be related to the environmental events in the South Atlantic that produced the *Braarudosphaera* chalk.

IGENOUS PETROLOGY AND GEOCHEMISTRY

At Site 564, basement rocks occur below 284 m sub-bottom depth. We drilled 81 m through a pillow basalt sequence cut by two minor massive lava flows. We recognized five lithologic units, which appear to belong to a single chemical group.

Lithology (Fig. 3)

Unit 3 (284.0–332.5 m)

Unit 3 consists of aphyric pillow basalts. We penetrated about 37 pillows, ranging from 20 to 150 cm in diameter with a mean thickness of about 75 cm. The pillows are separated from each other by black glass margins up to 3 cm thick. Aphanitic basalt close to the glass grades through a variolitic zone into fresh, fine-grained basalt pillow interiors. Up to 2% of clay-filled, subhedral-to-anhedral pseudomorphs of olivine microphenocrysts, ranging up to 2 mm in diameter, are present. Plagioclase laths, forming glomerophyric clusters up to 2 mm in diameter, are sparsely and randomly scattered.

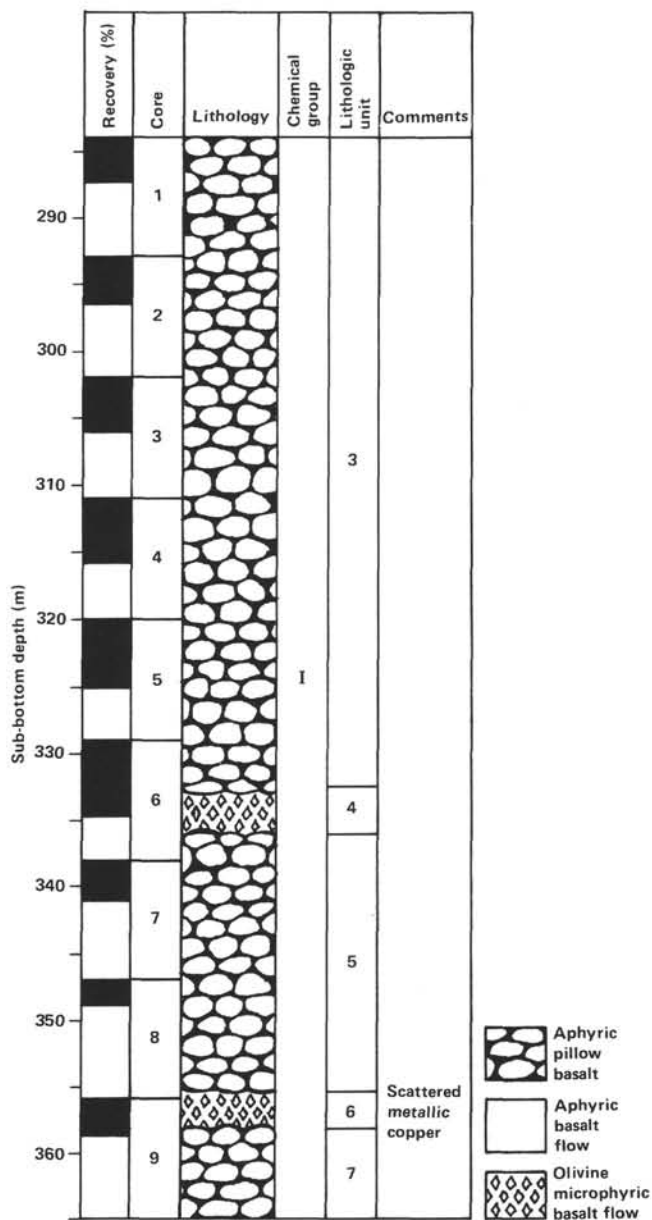


Figure 3. Basement lithology column, Hole 564.

Round and irregular vesicles are usually rare throughout the unit (less than 1%), but often show an increase in abundance close to upper pillow margins (2–3%). Most vesicles are empty, but if they are filled, calcite exceeds clay.

Interpillow breccia (hyaloclastite) was recovered in a few places. Black, angular-to-subrounded glass clasts occur either in a very pale brown limestone matrix or within a sparry calcite cement. Thin palagonite rinds on the glass are common throughout the section.

Unit 4 (332.5–336.5 m)

This unit (~4 m thick) consists of a massive aphyric basalt flow, containing a large amount of acicular plagioclase, ranging between 1 and 4 mm in length. Anedral olivine microphenocrysts are replaced by dark brown clay. The base of the flow is marked by variolitic basalt with a narrow rim of weathered glass.

Unit 5 (336.5–355.5 m)

This unit is composed of fine-grained aphyric pillow basalts with pillow sizes ranging between 40 and 70 cm. Black glassy pillow margins are often slightly altered to palagonite. Black brecciated basalt glass, embedded in limestone and/or calcite, occurs between many pillows.

Unit 6 (355.5 to 358.0 m)

Unit 6 is a massive, olivine microphyric basalt. The occurrence of a few chilled black glass pieces in the upper half suggests that it may consist of two separate flows. At the bottom, a chilled glass margin is present. The minimum thickness of Unit 6 is about 2.5 m.

Plagioclase laths up to 5mm long are abundant in most parts of Unit 6, but they seem to decrease in size downhole. Olivine phenocrysts, ranging in size between 0.5 and 1 mm, are mostly replaced by brown clay. Their abundance decreases from about 5% at the top to about 1% at the bottom.

Fractures and veins, usually horizontally oriented, are common. They are mostly cemented by calcite, but light green chlorite occurs on fracture planes in some places. In Unit 6 (Section 564-9-1) we found native copper, forming small needles and plates (0.5–4 mm in size).

Unit 7 (358.0–365.0 m)

We only recovered fragments of this lowermost unit, which consists of fine-grained, aphyric pillow basalts, topped by a basalt glass breccia. In the upper portion, two pieces are highly vesicular with round-to-oval vesicles up to 5 mm in diameter; these vesicles are either empty or filled with clay or calcite. Pieces with black glass rinds are also present.

Petrography

Ten thin sections were examined from this site. All are aphyric and all are similar in mineralogy, although there is some variation in olivine abundance. None of the lithologic units appears petrographically distinct, except that Unit 6 (Sample 564-9-1, 45–47 cm) appears more altered. Noteworthy is the occurrence of small

amounts of native copper in Sections 564-6-4 and 564-9-1.

Basalts of Site 564 are characterized by the presence, in varying proportions, of domains of contrasting grain size and texture. Both fine-grained and relatively coarse-grained domains are present, regardless of mean grain size or proximity to pillow or flow cooling surfaces. The relative abundance of coarse-grained domains appears to increase with increasing mean grain size.

Coarse domains range from isolated radiating clusters (10–15% of rock) surrounded by fine material, to continuous domains (60–70% of rock) surrounding circular or irregular, isolated fine-grained domains. Coarse domains are characterized by radiating clusters of hollow plagioclase laths (up to a maximum of 3 mm long) grading to randomly oriented aggregates in larger domains. Radiating clusters are frequently centered on one or more grains of olivine; relatively coarse, granular clinopyroxene fills the remaining interstices. Within these domains textures are intergranular or subophitic. Olivine, generally about 5% but ranging from 1 to 10% in abundance, is largely confined to these domains. It occurs as diamond-shaped, pseudo-hexagonal, or anedral microphenocrysts and is seldom fresh, being altered to aggregates to pleochroic green montmorillonite (e.g., Section 564-6-4), green brown clay or, in some cases (e.g., Sample 564-5-3, 119–122 cm), to light brown zeolite similar to (?) heulandite of Site 559.

Fine domains are dominated by sheaflike or branching aggregates of clinopyroxene with an equal proportion of plagioclase occurring as interstitial patches, small laths, or (less commonly) plumose aggregates. Interstitial glass, colorless when fresh, crowded with extremely fine opaques and skeletal magnetite, and frequently altered to clay or zeolite, forms up to 15% of these domains. Granular magnetite (5–8% of rock) is largely confined to fine domains.

The precise cooling history of these unusual rocks is difficult to interpret in detail. However, it is clear that olivine and plagioclase were crystallizing together at an early, probably pre-eruptive, stage. Plagioclase continued to crystallize without further olivine after eruption-forming coarse domains. Final crystallization of clinopyroxene, plagioclase, and magnetite together formed the fine domains.

Alteration has had varying effects throughout the hole. Most samples show small amounts of brown or orange clay attributable to weathering. Zeolite, similar to heulandite identified at Site 559, has replaced olivine and glass in most samples. Montmorillonite, pleochroic from green to pale green or yellow, with $2V_x$ approximately 10° and occurring as relatively large (up to about 0.2 mm) single grains or optically continuous aggregates is also present replacing olivine in several samples. Traces of pyrrhotite and native copper occur in Sample 564-6-4, 44–46 cm. In Section 564-9-1 visible native copper occurs as scattered small granules within about 1 cm of small calcite-filled and chlorite-filled veinlets. A thin section from one such occurrence (Sample 564-9-1, 45–47 cm) contains up to 20% altered material; glass has

been altered to a mixture of green and brown clays and possibly chlorite. Olivine has been altered to near-opaque to dark brown hematite and (?)goethite along with brown clay and calcite. Pyrrhotite is also present in trace amounts in this specimen.

Geochemistry

Twenty-six samples have been analyzed from Hole 564; the analyses are presented in Table 2, and selected elements are plotted against sub-bottom depth in Figure 4.

The analyzed basalts appear to compose a single chemical group, although there is apparent chemical variation downhole for some elements within this group. Table 3 contains the average analysis of 20 fresh basalts from Hole 564, together with average analyses for the six uppermost and six lowermost basalts in the hole. The average analysis for all fresh basalts suggests that much of the chemical variation may lie within analytical precision. However, the average analyses for uppermost and lowermost fresh basalts in Table 3 do indicate some significant differences, notably an increase in Fe_2O_3 , TiO_2 , Zr, Nb, and perhaps MgO abundances, and a decrease in Al_2O_3 and CaO abundances and Zr/Nb ratio downhole. The reported Nb values all lie within a factor of three times the analytical precision. For all elements, the downhole chemical gradient is continuous, making it impossible to define chemical subgroups.

In comparison to the fresh basalts, the altered basalts analyzed (Table 3) display chemical changes consistent with those described for altered basalts from Sites 559

and 562. The abundances of, particularly, Zr and Nb, and the value of the Nb/Zr ratio, do not change upon alteration (Table 3). Thus, the apparent increase in Zr and Nb content and in Nb/Zr ratio downhole cannot be correlated with secondary processes (such as degree of alteration) or with simple primary processes (such as variation in phenocryst content). At this stage, the significance of the downhole chemical gradient is uncertain.

Plotted on a modified Coryell-Masuda diagram (Fig. 5), all of the basalts from Hole 564 have depleted trace element characteristics. However, Figure 5 also illustrates the less depleted nature of the basalts from the deepest levels of the hole ($[\text{Nb}/\text{Zr}]_{\text{ch}} \sim 0.54$).

MAGNETICS

Oriented minicores were taken for on-board study of paleomagnetic properties. After measuring the natural remanent magnetization (NRM) and initial susceptibility, a few samples were subjected to alternating field (AF) demagnetization. Typical results of AF demagnetization are plotted in Figure 6. An orthogonal plot of the components of magnetization (Fig. 6) suggests the presence of univectorial direction, with shallow downward inclination value. Median demagnetizing field (MDF) is calculated using Figure 6. The detailed results of AF demagnetization, NRM, and susceptibility are given in Table 4.

The stable inclination and susceptibility values are plotted versus depth on Figure 7. All samples have shallower inclination values compared to the samples from previous holes, and the values are more shallow than the

Table 2. Analyses of major elements (in wt.%) and trace elements (in ppm) of Hole 564 basalts.

Core-Section (interval in cm) (piece number)	Sub- bottom depth (m)	SiO ₂	TiO ₂	Al ₂ O ₃	Fe ₂ O ₃	MnO	MgO	CaO	K ₂ O	P ₂ O ₅	Total	Mg'	Ti	V	Sr	Y	Zr	Nb
1-1, 108-111 (10A)	285.1	50.48	1.42	14.68	11.05	0.16	7.16	12.09	0.27	0.17	97.48	59	8250	385	112	39.0	89	3.4
1-1, 140-143 (12A)	285.4	50.77	1.44	14.53	11.05	0.17	7.26	12.10	0.34	0.15	97.81	60	8640	413	108	42.0	91	3.3
1-2, 74-78 (5D)	286.3	49.85	1.43	14.89	11.99	0.18	7.06	12.13	0.26	0.14	97.93	57	8580	397	106	39.0	89	3.6
1-3, 103-105 (8B)	288.0	49.37	1.45	15.02	12.33	0.16	5.98	12.48	0.29	0.14	97.22	52	8700	403	104	39.6	92	4.0
2-1, 53-55 (4B)	293.6	48.81	1.46	15.28	12.50	0.18	6.13	12.47	0.19	0.15	97.17	52	8760	426	107	37.3	90	3.4
2-2, 46-49 (3B)	295.0	49.49	1.42	14.62	11.80	0.17	6.93	12.05	0.31	0.14	96.93	57	8520	378	102	38.2	88	3.2
2-3, 60-63 (5)	296.6	49.67	1.41	14.45	11.87	0.17	7.75	11.98	0.24	0.14	97.68	60	8460	380	106	38.4	94	4.3
3-1, 25-28 (2B)	302.3	50.09	1.42	14.42	11.69	0.17	7.09	12.00	0.28	0.15	97.31	58	8520	372	105	39.7	89	2.8
3-2, 70-73 (5C)	304.3	48.75	1.45	14.76	12.14	0.18	6.46	12.43	0.26	0.15	96.58	55	8700	396	106	40.0	88	3.9
3-3, 138-141 (8B)	306.4	50.65	1.42	14.46	11.67	0.16	6.84	11.86	0.15	0.14	97.35	57	8520	377	107	38.6	92	4.6
4-1, 61-65 (4C)	311.6	50.14	1.41	14.26	11.57	0.17	7.54	11.80	0.26	0.15	97.30	59	8460	376	106	38.6	85	5.6
4-2, 102-106 (6A)	313.5	49.67	1.43	14.61	11.81	0.18	7.14	11.94	0.28	0.15	97.21	58	8580	394	106	40.4	89	3.9
4-4, 81-85 (3C)	316.4	50.33	1.43	14.53	11.78	0.17	7.07	11.81	0.34	0.15	97.61	57	8580	345	104	41.6	86	4.6
5-1, 17-19 (1E)	320.2	49.26	1.47	14.99	12.08	0.18	6.42	12.16	0.25	0.15	96.96	54	8820	405	105	40.3	90	5.4
5-2, 98-100 (4B)	322.5	50.67	1.44	14.44	11.85	0.18	7.56	11.79	0.13	0.16	98.22	59	8640	383	98	39.2	95	4.8
5-3, 119-122 (5G)	324.2	50.44	1.45	14.47	11.03	0.19	7.81	11.84	0.20	0.15	97.58	61	8700	424	118	40.2	97	4.5
6-1, 33-36 (1B)	329.4	50.33	1.45	14.32	12.11	0.17	7.55	11.72	0.06	0.15	97.86	58	8700	392	101	40.3	97	5.6
6-3, 63-66 (5A)	332.6	49.81	1.45	14.24	12.18	0.18	7.41	11.52	0.37	0.14	97.30	58	8700	388	102	40.7	87	5.5
6-4, 44-47 (2D)	334.0	49.56	1.42	14.25	11.88	0.18	8.25	11.54	0.18	0.15	97.41	61	8520	383	99	38.4	93	4.5
6-5, 43-46 (1J)	335.5	50.61	1.49	14.40	11.55	0.18	7.20	11.74	0.22	0.15	97.54	58	8940	385	103	40.3	98	6.0
7-2, 20-23 (1D)	339.7	49.63	1.49	14.41	12.31	0.18	7.15	11.75	0.31	0.16	97.39	57	8940	398	104	42.3	98	5.4
7-3, 58-61 (4C)	341.6	50.21	1.47	14.03	12.11	0.18	7.62	11.60	0.18	0.15	97.55	59	8820	378	108	41.6	96	5.5
8-2, 0-3 (1A)	348.5	50.12	1.47	14.24	12.21	0.17	7.38	11.60	0.35	0.13	97.67	58	8820	378	108	40.9	96	6.0
8-2, 75-77 (7)	349.3	48.66	1.50	14.94	12.92	0.18	5.94	11.98	0.24	0.17	96.53	51	9000	463	109	42.4	96	6.1
9-1, 43-45 (1D)	356.5	49.29	1.47	14.61	12.61	0.18	6.59	11.96	0.31	0.15	97.17	54	8820	463	108	42.5	99	5.4
9-3, 72-75 (4B)	358.3	49.75	1.46	14.05	12.25	0.19	7.40	11.49	0.16	0.15	96.90	58	8760	375	102	40.8	100	4.6

a On-board measurements were made on ignited samples. Onshore analyses of loss on ignition are less than 1% in most cases. Compiled data tables at the end of this volume (Appendix) include volatile components.

b Total Fe as Fe_2O_3 .

c Mg' is the atomic ratio of $100 \times (\text{Mg}/[\text{Mg} + \text{Fe}^{2+}])$; calculated using an assumed $\text{Fe}_2\text{O}_3/\text{FeO}$ ratio of 0.15.

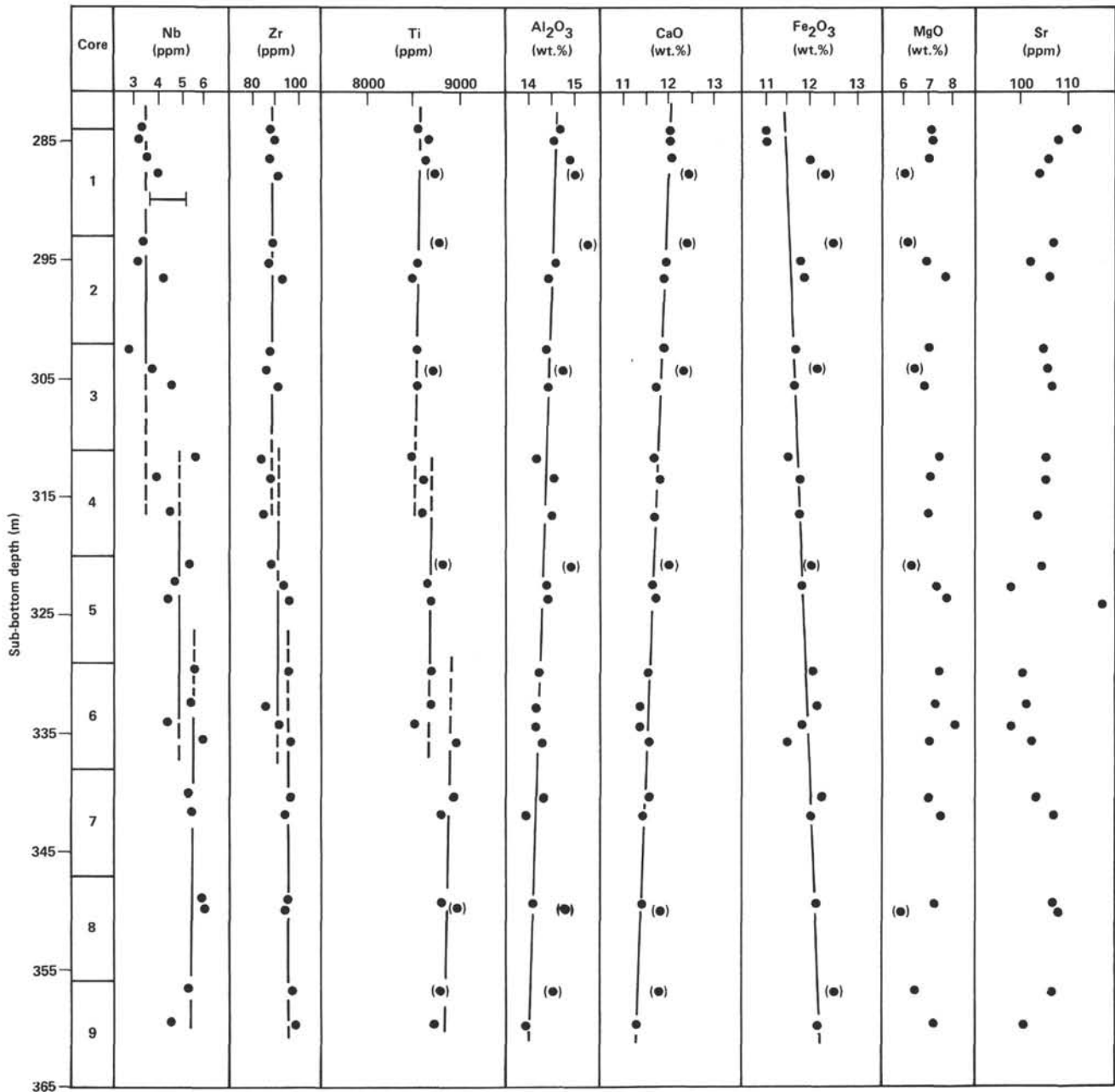


Figure 4. Downhole variations in chemical abundances, Hole 564. Symbols in parentheses indicate concentrations affected by alteration.

expected dipole inclination value for the latitude of this site. This may be due to tectonic rotation of the crust since the acquisition of magnetization by these basalts.

PHYSICAL PROPERTIES

A section of 81 m was cored through basalt basement. Lithologies include massive, glassy, and vesicular basalts and hyaloclastic breccias. Physical measurements could not be obtained for the breccias because the clasts were commonly 10 mm across, and a representative bulk sample of a suitably small size for laboratory measurements was not available.

All the samples measured were basalts, which make up the vast majority of the recovered material. Sonic ve-

locities, bulk densities, and porosities were determined by the standard DSDP methods (see Explanatory Notes, this volume), and the results are presented in Table 5 and Figure 8. The data have a scattered distribution, shown on the expanded plot scales of Figure 8. There is an apparent variation of properties downhole with a peak in velocity at about 295 m followed by a gradual decrease to 315 m. This is almost certainly an artifact of the sampling, because much greater variability is seen where the sampling density is higher between 320 and 340 m sub-bottom. In this section, samples taken from within a few centimeters of each other for the separate determination of vertical and horizontal velocities show large differences that are not attributable to systematic seismic anisotropy down the section.

Table 3. Average analyses of basalts from Hole 564.

Element	Fresh basalts		Altered basalts		Uppermost 6 fresh basalts		Lowermost 6 fresh basalts	
	\bar{X}	σ	\bar{X}	σ	\bar{X}	σ	\bar{X}	σ
Major elements (wt.%)								
SiO ₂	50.11	0.40	49.02	0.29	50.06	0.45	49.98	0.37
TiO ₂	1.44	0.02	1.47	0.02	1.42	0.01	1.47	0.02
Al ₂ O ₃	14.42	0.20	14.93	0.21	14.60	0.16	14.23	0.15
Fe ₂ O ₃	11.79	0.38	12.43	0.29	11.58	0.38	12.05	0.26
MnO	0.18	0.01	0.18	0.01	0.17	0.01	0.18	0.01
MgO	7.36	0.33	6.25	0.25	7.21	0.26	7.50	0.37
CaO	11.82	0.20	12.25	0.22	12.06	0.05	11.62	0.10
K ₂ O	0.24	0.08	0.26	0.04	0.28	0.03	0.23	0.07
P ₂ O ₅	0.15	0.01	0.15	0.01	0.15	0.01	0.15	0.01
Mg'	58	1	53	1	58	1	59	1
Trace elements (ppm)								
V	385	16	426	28	388	14	383	8
Sr	105	4	107	2	107	3	104	3
Y	40.00	1.30	40.40	1.80	39.40	1.20	40.70	1.20
Zr	92	4	93	4	90	2	97	2
Nb	4.60	1.00	4.70	1.00	3.40	0.50	5.30	0.60
(Nb/Zr) _{ch}	0.46	0.11	0.46	0.09	0.36	0.04	0.54	0.06

Note: Averages of 20 fresh basalts and 6 altered basalts are calculated from data presented in Table 2. The altered basalts are samples from Sections 564-1-3, 564-2-1, 564-3-2, 564-5-1, and 564-9-1 and from Sample 564-8-2, 75-77 cm. \bar{X} is mean; σ is standard deviation; Mg' is the atomic ratio of $100 \times (\text{Mg}/[\text{Mg} + \text{Fe}^{2+}])$, calculated assuming an Fe₂O₃ ratio of 0.15.

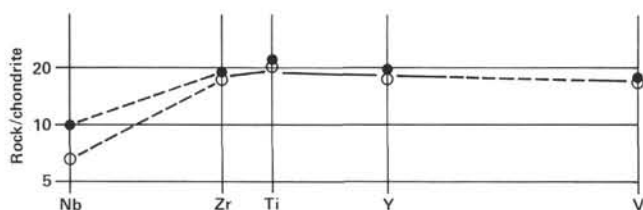


Figure 5. Extended Coryell-Masuda diagrams for basalts of Hole 564. Solid circles are average of lowermost six fresh basalts: $(\text{Nb}/\text{Zr})_{\text{ch}} \sim 0.36$. Open circles are average of uppermost six fresh basalts: $(\text{Nb}/\text{Zr})_{\text{ch}} \sim 0.54$.

Also apparent in Figure 8 is a negative correlation between density and seismic velocity, which is the inverse of the usual relationship. The bulk densities were determined while the ship was in moderately heavy seas, and weighing errors account for this unusual negative correlation.

DOWNHOLE MEASUREMENTS

Logging

Operations

Logging operations were started at 1530Z, 30 October with the intention of making as many logs as possible before the arrival of a predicted tropical storm. Because it seemed likely that bad weather would necessitate an early termination of operations, the order of the logging runs was changed so that the resistivity log, which has consistently given the best results, was first. We originally planned to run the porosity/density logs second, the sonic third and, if weather permitted, the high resolution temperature sonde (HRT) last. However, after the resistivity and porosity/density logs had been

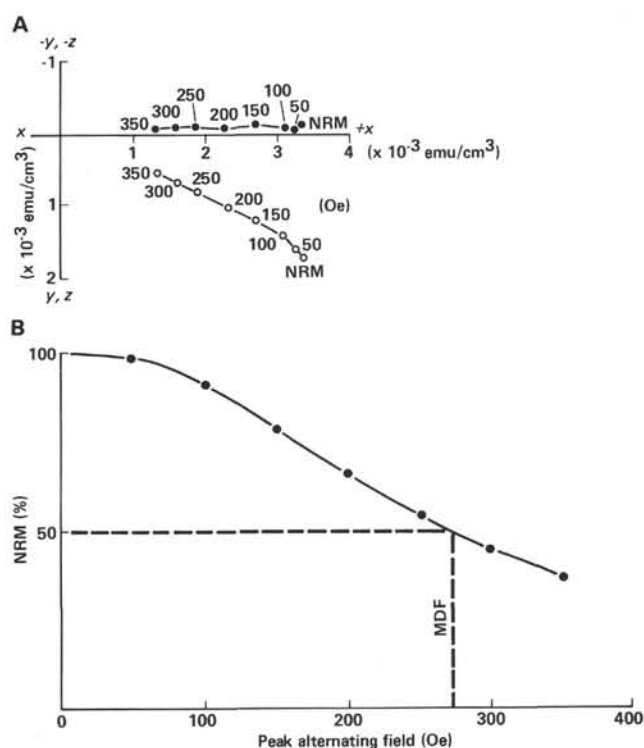


Figure 6. A. Vector diagram showing change in NRM after alternating field demagnetization (Sample 564-3-1, 39-41 cm). Solid circles are plotted on the horizontal plane and open circles are plotted on the vertical plane. B. Percent natural remanent magnetization (NRM) versus peak alternating field with the determination of median demagnetizing field (MDF).

run, the predicted storm had not developed. Because there was not enough time to carry out a piston coring program, we decided to make two runs with the temperature probe.

Hole conditions were generally good. The amount of heave was the lowest of all three holes logged during this leg. High quality records were obtained for all logging runs despite minor problems with the caliper log and the porosity/density tool, which consumed about 1 1/2 additional hours. Because of problems at the previous two logged holes in lowering the HRT down the hole, the tool was weighted by being placed inside a perforated core barrel. This modification is described in detail in the Downhole Temperatures section. A schedule of logging runs is given in Table 6.

Sedimentary Section

All tools were logged continuously from the basement interface to the drill pipe at 100 m sub-bottom. The data quality is regarded as good because of the low sea state and good hole condition. In particular, the hole was not washed out beyond the limits of the sonic caliper (16 in.) and a full caliper log was recorded. Below 130 m sub-bottom, the maximum diameter is only 14 in., and although this is slightly greater than the reach of the density/porosity excentralizer (13 in.) this tool was very close to the hole wall, if not in contact with it, for most of the logged section. The density log contains more detail and less random noise than in Holes 556 or 558, but because

Table 4. Hole 564 basalt paleomagnetism.

Core-Section (interval in cm)	J _{NRM} (× 10 ⁻³ emu/cm ³)	NRM inc. (°)	Stable inc. (°)	χ (× 10 ⁻⁶ emu/cm ³ Oe)
3-1, 39-41	3.75	26.8	22.6	180
3-2, 35-37	3.47	19.3	17.0	76
3-2, 90-92	4.13	20.5	18.5	85
3-2, 129-131	2.39	36.0	27.1	70
3-3, 36-38	4.63	17.0	15.8	90
4-1, 7-9	3.13	28.2	21.8	115
4-2, 37-41	3.40	13.2	11.9	115
4-2, 49-51	2.30	36.9	30.5	105
4-3, 4-6	2.82	10.7	7.3	125
4-3, 137-139	2.16	9.6	9.4	117
4-4, 3-5	4.01	14.1	12.5	134
4-4, 78-80	2.38	24.0	19.9	115
4-4, 140-142	2.80	15.3	11.8	130
5-1, 6-8	4.04	26.4	20.7	160
5-1, 81-83	4.26	26.4	25.6	113
5-2, 31-33	2.88	16.1	11.7	120
5-3, 95-97	2.41	29.8	25.6	160
5-4, 144-146	1.55	17.8	17.1	161
5-5, 27-29	4.18	7.2	7.2	135
6-1, 26-28	5.71	28.3	15.6	234
6-2, 48-50	2.92	45.3	33.3	160
6-3, 145-147	2.31	50.4	31.0	166
6-4, 123-125	5.87	36.8	14.6	318
6-5, 32-34	3.18	20.9	12.3	124
7-2, 11-13	3.45	27.3	23.7	127
7-3, 102-104	1.89	24.5	13.1	167
8-1, 41-43	3.31	23.6	21.2	128
9-1, 8-10	4.36	31.1	21.7	384
9-2, 128-130	2.69	26.1	19.7	204
9-2, 142-144	0.59	44.1	25.1	142

Note: J_{NRM} = intensity of natural remanent magnetization (NRM); inc. = inclination; χ = susceptibility.

it contains obvious noise spikes, it is drawn dashed in Figure 9, which compares density, velocity, resistivity, and natural gamma logs.

As was noted in the physical property measurements, there is no boundary within the sediments as clearly defined as the boundaries at Holes 556 and 558, although a gradational rise in velocity and density superimposed on the background compaction gradient can be seen over

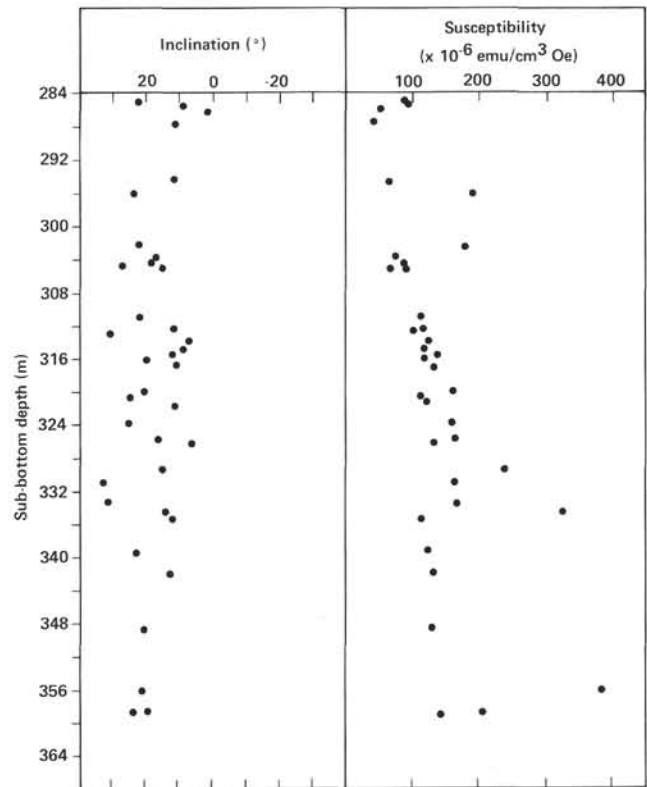


Figure 7. Downhole plot of stable inclinations and susceptibility of Site 564 basalts. (Values between 284 and 300 m sub-bottom are not listed in Table 4.)

the depth range 160-200 m. Over this range the sedimentology changes character as described in the Sedimentology and Biostratigraphy section. Density, sonic velocity, natural gamma, and resistivity values all increase from 270-285 m sub-bottom towards the base-

Table 5. Physical properties measurements, Hole 564.

Core-Section (interval in cm)	Sub-bottom depth (m)	Sonic velocity (km/s)		Temperature (°C)	Gravimetric density			Lithology or remarks
		V.	H.		Wet-bulk density (g/cm ³)	Water content (%)	φ (%)	
1-1, 35-40	284.4		5.28	23				All samples basalt
1-1, 112-114	285.1	5.12		23				
1-3, 18-20	287.2	5.52		23	2.88	2	6	
1-3, 23-27	287.2		5.43	23				
2-2, 16-21	294.7	5.92		23	2.81	3	9	
3-2, 121-131	304.8	5.56	5.26	23	2.82	3	9	
4-2, 37-41	312.9	5.27		23	2.87	2	5	
5-2, 44-56	322.0	5.05		24				
5-2, 51-57	322.0		5.39	24	2.87	2	5	
5-3, 68-75	323.7		5.25	24	2.86	2	7	
5-3, 82-84	323.8	5.77		24				
6-1, 11-13	329.1	5.73		24				
6-1, 80-90	329.8		4.88	24	2.76	4	12	Vesicular basalt
6-4, 48-52	334.0	5.31		24				
7-1, 139-143	339.4	5.68		24				
7-3, 13-15	341.1	6.17		24				
7-3, 51-55	341.5		5.62	24	2.88	1	4	All samples basalt
8-2, 76-85	349.3	4.83	4.74	24	2.80	5	13	
9-1, 25-35	356.3	5.07	4.87	24	2.84	3	10	

Note: V. = vertical, H. = horizontal; water content is corrected; φ = porosity. Weighing accuracy below average because of rough seas.

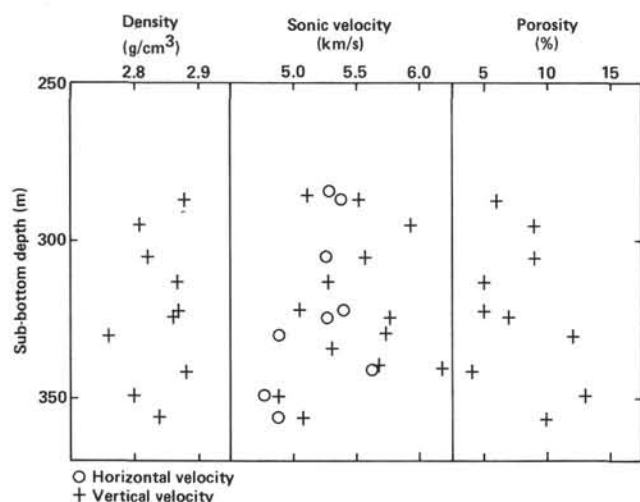


Figure 8. Selected physical property variations in the basement rocks of Hole 564.

Table 6. Schedule of logging runs.

Run 1. Dual laterolog (DLT), gamma ray (GR), caliper (CAL) Logger on bottom 2045 10/30
Run 2. Formation density compensated (FGT), neutron porosity (CNT), GR, CAL Logger on bottom 0330 10/31 Remarks: Three repeat sections made to observe variations caused by heave.
Run 3. High resolution temperature (HRT) #1 Logger on bottom 1000 10/31 Remarks: Sonde mounted inside modified core barrel to provide extra weight. Tool stood up at 4115 m, 4158 m, 4172 m; stationary measurements at 4135 m, 4178 m, 3830 m.
Run 4. Sonic velocity (DDBHC), GR, CAL Logger on bottom 1500 10/31 Remarks: Transit time and waveform recordings both repeated. Waveform in basement only.
Run 5. HRT #2 Logger on bottom: 2030 10/31 Remarks: Sonde mounted inside modified core barrel. Tool stood up at 4158 m, 4172 m; stationary measurements at 3815 m, 4158 m, 4170 m.

Note: Circulation stopped: 1600 hr. 30 October.

ment interface, probably because of a dolomitized layer as seen at Sites 558 and 563.

The most interesting feature of the logs is a cyclic variation in values with a wavelength of about 10 m within the depth range 180–230 m. Three prominent peaks in these cycles are shown by dashed lines in Figure 9. This variation was tentatively identified by physical property measurements at Site 563 and probably correlates with alternations of chalk and ooze as described in the sedimentology of the core section of Site 563. This cyclic variation makes the identification of a distinct sedimentologic boundary problematic. The best limits are those defined above (the depth range 160–200 m).

Basement Section

The results of logging within basement are shown in Figure 10. Each of the four major logs represents the average, by eye, of two or more passes through the basement.

The general character of the logs recorded in the basement is more uniform than that of the logs of the pre-

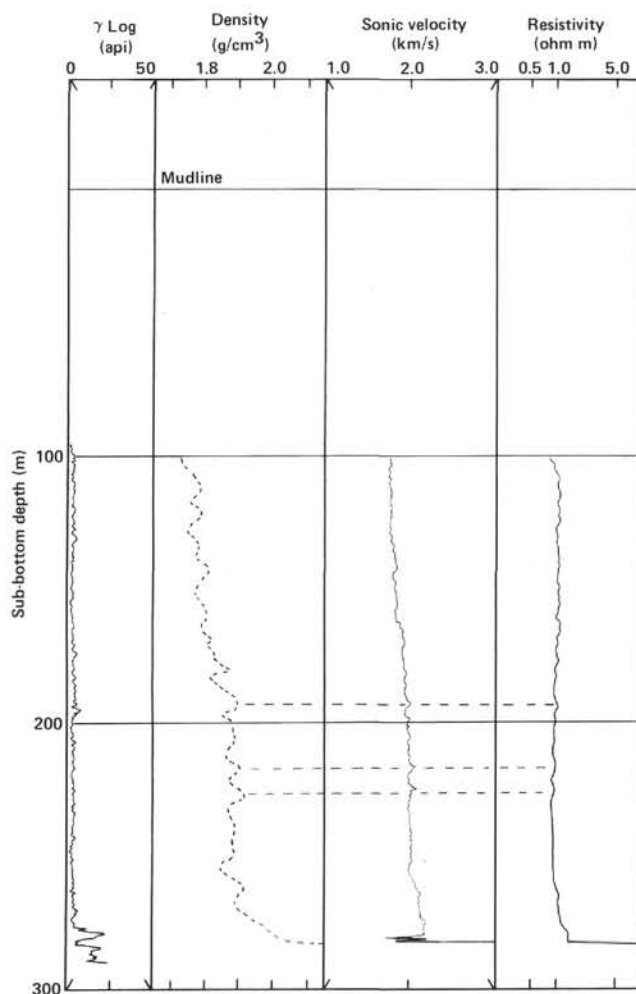


Figure 9. Wireline log curves for sedimentary section of Hole 564. Dashed density curve indicates low quality data. Dashed horizontal lines mark cyclical peaks discussed in text.

vious two logged holes. This is particularly true of the resistivity log, which is remarkably uniform from the sediment/basement interface down to a depth of 320 m sub-bottom. This relatively uniform character correlates with the thick layer of pillow basalts, Unit 3, at the top of the basement. A narrow interval between 330 and 336 m sub-bottom of high sonic velocity, high density, low porosity, and high resistivity corresponds to the massive basalt flow, Unit 4. This unit is shown by a vertical bar in Figure 10.

The porosity and density logs show several zones 2 to 4 m wide of high porosity and low density indicated by the speckled bands in Figure 10. To a lesser extent, these intervals correspond to anomalies in the resistivity and sonic velocity profiles. These low porosity zones reflect interpillow sediments and/or gaps and crevices that cannot be detected by drilling. The deepest of these high porosity zones, between 328 and 332 m sub-bottom, may correspond to the "thief zone" that has been inferred from the downhole temperature measurements. This high porosity zone also corresponds to the largest low-resistivity anomaly recorded within basement.

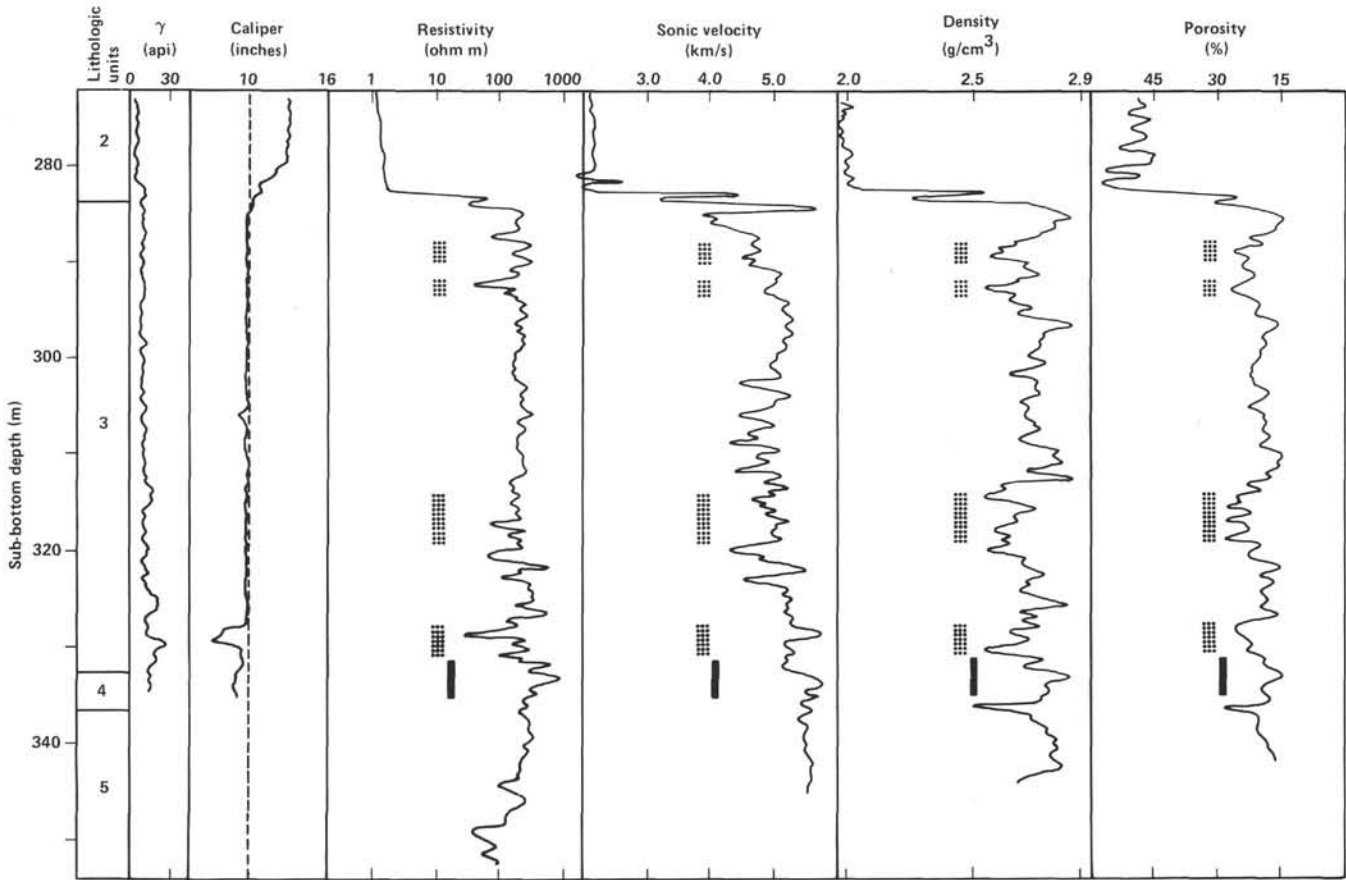


Figure 10. Wireline log curves for basement section of Hole 564. Curves have been redrawn omitting noise spikes. Gaps indicate intervals where noise obscures data. Speckled bands mark zones of high porosity and low density discussed in text. Vertical bar between 330 and 336 m sub-bottom depth marks the zone of high sonic velocity discussed in text.

It is not clear whether or not the high-amplitude, short-wavelength (about 1 m) variations observed in all four logs at the sediment/basement interface are real. These short-wavelength variations show up consistently on nearly every pass of the tools and also correspond to short-period variations in the drilling rate, suggesting that there is a very thin sedimentary layer just below the top of basement. However, the width of this feature is so small that the variation might also be due to the effect of heave on the tool as it crosses the sediment/basement interface. The wavelength of the heave is identical to the wavelength of the observed variation.

Downhole Temperatures

The data from the two HRT runs, recorded logging down the hole, are shown in Figure 11. The HRT tool was modified by encasing it in a modified core barrel as shown in Figure 12. The increased tool weight was sufficient to allow detection of setdown by the logging winch tension meter. On both runs it was necessary to spud the tool through blockages within the basement, and both times, after this the response of the tool was very slow, apparently because of mud packed around the thermistor, so that no useful data were obtained by logging back up the hole. However, by the time the tool was back up at the mudline, its response had returned to

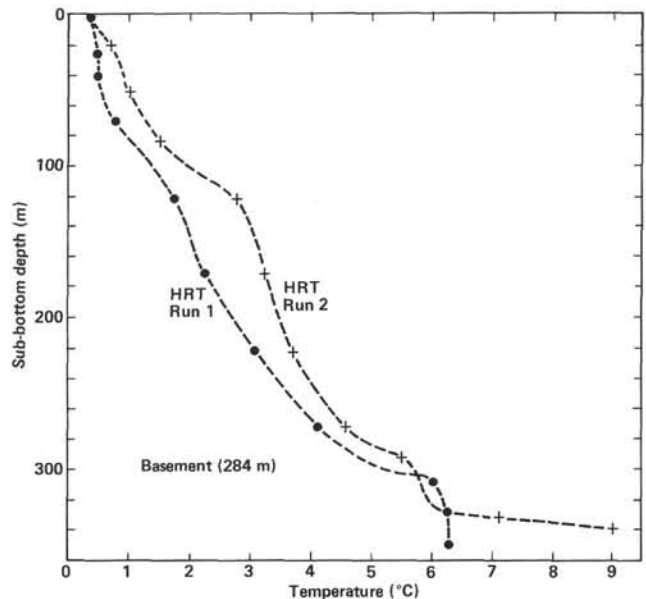


Figure 11. High resolution temperature (HRT) log curves for Hole 564. For explanation see text.

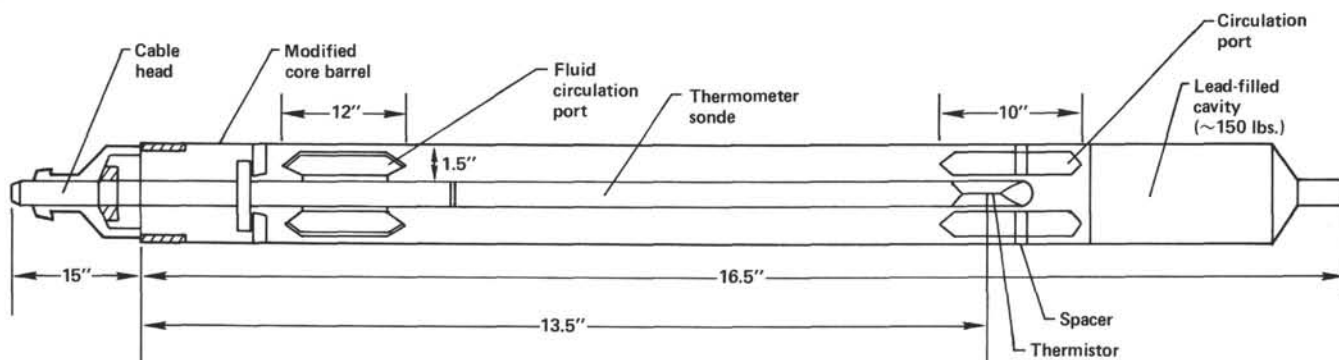


Figure 12. Schematic diagram of high resolution temperature sonde with weight-adaptor modification. Diameter = 3 5/8 in.; total weight = 300 lbs.

normal. The important result of the two runs is the discovery of an equilibrated temperature profile with a very low gradient ($4^{\circ}\text{C}/\text{km}$) in the range of 190 to 300 m sub-bottom as shown by the identical profiles on the two runs.

During logging the bottom of the drill pipe was moved between the depths of 3960 and 3930 m (100 and 130 m sub-bottom). The disparity in the two profiles centers on fluctuations at these depths and it is concluded that these are due to the interaction of the end of the drill pipe and the sidewall of the hole.

Within the basement, the temperature gradient is higher and more variable. Below 328 m sub-bottom, temperature measurement was difficult because of mud covering the thermistor, and temperatures were determined by allowing the tool to equilibrate at constant depth. The values thus determined define a very high temperature gradient of $250^{\circ}\text{C}/\text{km}$ between 328 and 340 m sub-bottom. These data can be explained by downflow of seawater to below the sediment/basement interface producing the steady, low-temperature gradient within the sediments. The water must escape from the hole through a "thief zone" above the section with the high temperature gradient, and it probably does so through one or more of the high porosity zones identified in the well logs in Figure 10.

The rate of waterflow must be less than that at Site 556, where the temperature gradient within the sediments was immeasurably low (less than $1^{\circ}\text{C}/\text{km}$). The importance of temperature measurements at Sites 556 and this hole is the demonstration that the drawdown of seawater is a common, if not essential, feature of the ocean crust when the overlying sediment blanket is pierced.

Ocean-Water Profile

The ocean-water temperature profile (Fig. 13) was logged through the drill pipe as the HRT tool was being recovered after the first run.

Below 1700 m, the profile is nearly identical to that at Site 558, slowly decreasing from 2.5°C to a similar rather cold bottom temperature of 0.4°C . Above 1700 m the temperature gradient is higher, the temperature rising in a linear manner to 18°C at 80 m depth. Above this there is a very sharp rise in temperature within the surface water layer to 23°C .

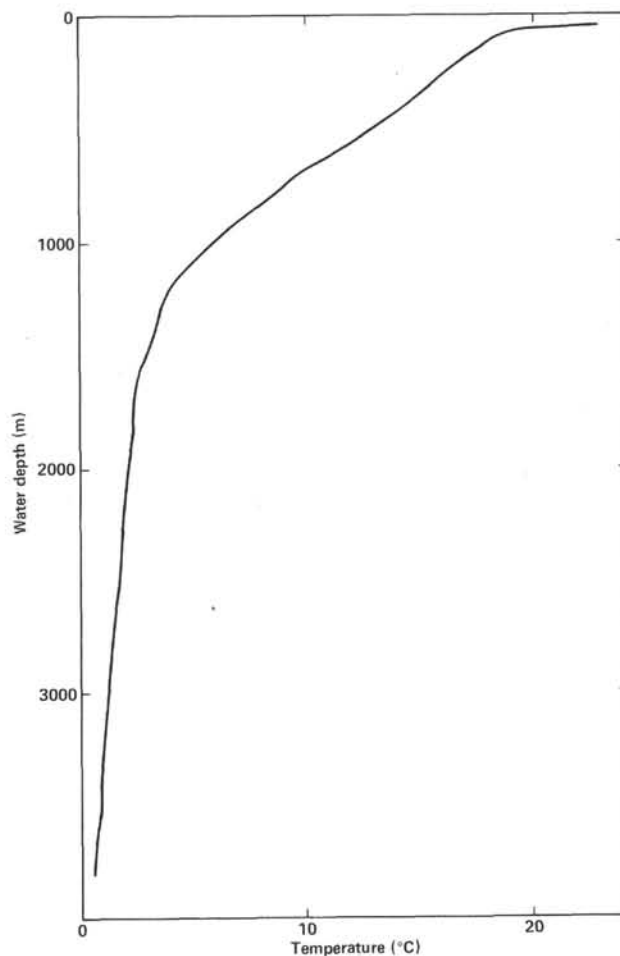


Figure 13. Ocean temperature profile recorded by high resolution temperature log within drill pipe.

This profile clearly defines three distinct layers within the ocean water and contains a detailed record of their boundaries. The drill string is regarded as being in equilibrium with the water at any depth because, although its conductivity is high, the temperature gradients along it are low. Also because of the low gradient, the temperature can be logged at the normal tool speed in drill string of 10,000 ft./hr. Thus good oceanographic data

are obtained for no cost, and we suggest that ocean temperature logs be made for all future DSDP logged holes.

SUMMARY AND CONCLUSIONS

The poor penetration into the basement and the single petrographic unit recovered at Site 563 necessitated the drilling of another site nearby to document better this area south of the Hayes Fracture Zone. After the results obtained north of the Hayes Fracture Zone where depleted and enriched basalts were found at two sites (558 and 561), it was important to have the most extensive sampling program possible south of the Hayes Fracture Zone.

The sediments were washed down to the basement, which was cored for 81 m. The basement consists of a single petrographic unit of aphyric basalts forming pillows (fresh glass were recovered from the top to the bottom of the hole); two massive flows about 2 m thick were also identified. Chemically, the recovered samples form one single group even though a gradient is observed from the top to the bottom. CaO, for example, varies in a continuous way from 12% at the top to 11.5% at the bottom with very little scattering. Concentration gradients are also observed for the magmaphile elements; it may be that the Nb/Zr ratio is not constant from the top to the bottom but such a possible variation will have to be confirmed onshore by measurements of La and Ta concentrations, because the variations recorded in Nb are less than three times the estimated precision.

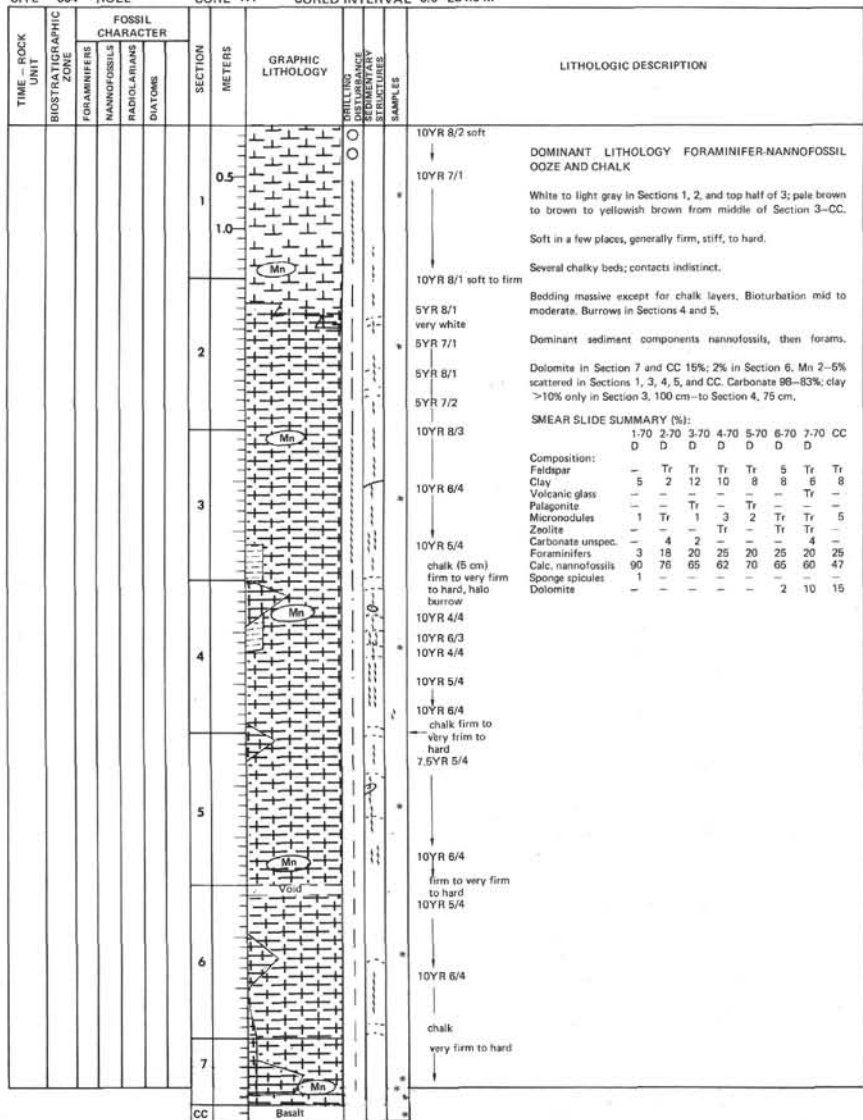
In terms of $(\text{Nb}/\text{Zr})_{\text{ch}}$ ratio, varying from 0.36 to 0.54, the basalts at this site are depleted. In terms of rare earths, the patterns may range from depleted to flat

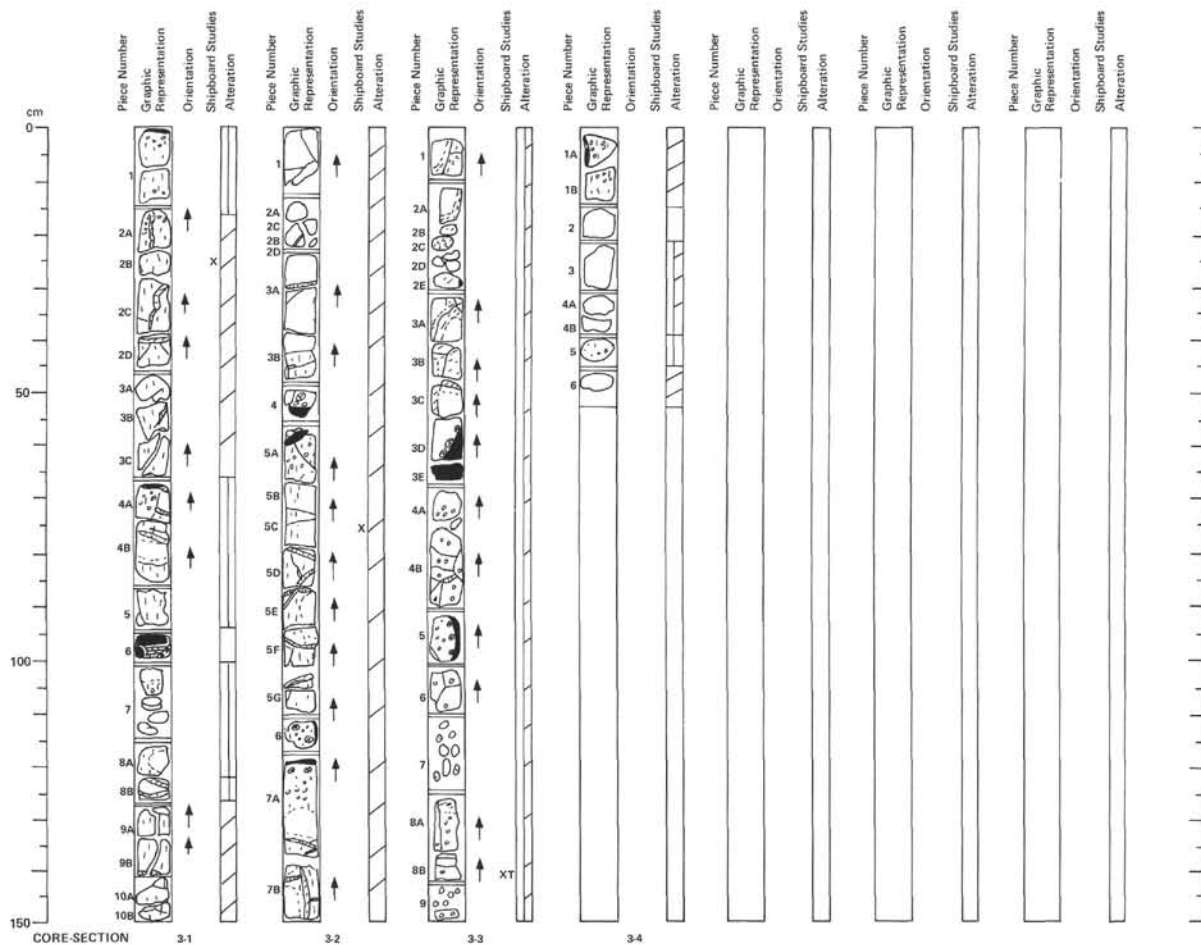
according to the value of Nb/La ratio; onshore measurements are necessary.

Considering the enrichment or depletion of the most magmaphile elements compared to the less magmaphile elements, previous researchers had shown that, at zero age, a boundary exists at the latitude of the Hayes Fracture Zone between "Azores" abnormal basalts and typical MORB (see Background and Objectives section). With respect to such a boundary, only depleted material was recovered from the drilled holes on Anomalies 6 and 13 south of the Hayes Fracture Zone, whereas both enriched and depleted materials were recovered from the holes north of the Hayes Fracture Zone; it was also found that depleted and enriched basalts may occur at a single site. Because these results do not fulfill entirely the hypotheses made before the cruise and because more fundamental geochemical problems have been encountered, additional data—*isotopic ratios and other magmaphile element determinations*—are necessary before any further geochemical mantle sources—*geodynamical interpretations* are possible.

A complete set of logs was run at Site 564. The most important result probably concerns the temperature logs. Two temperature profiles were recorded, the first one 18 hr. after circulation was stopped and the second 10 hr. later to see if the hole had achieved equilibrium. The two profiles were identical down to below the sediment/basement interface showing a low gradient of about 4°C/km, which is only a fraction of the normal gradient. Between 45 and 60 m in the basement, an increase of 2.5°C was observed. This provides additional evidence at Anomaly 13 of downflow of seawater when the sedimentary layer is pierced.

SITE 564 HOLE CORE H1 CORED INTERVAL 0.0-284.0 m





SITE 564, CORE 3

Depth 302.0-311.0 m

SECTION 1

APHYRIC PILLOW BASALT

16-66, 101-121, and 129-150 cm: Fine grained, gray (2.5Y N5) aphyric pillow basalt moderately altered to light yellowish brown (2.5Y 6/4) along pillow margins.

16-20 cm: ~1% round calcite filled vesicles at altered pillow margins (1-2 mm diameter).

35-40 cm: <1% irregular vesicles (1-3 mm) filled with dark green clay(?). Calcite in fractures.

0-15, 30-94, and 122-126 cm: Aphyric basalt as above but more highly altered to light yellowish brown (2.5Y 6/4) throughout. 2-3% round and irregular empty vesicles (1-2 mm), especially near pillow margins. Calcite in fractures.

0-1, 68 and 68-69 cm: Glass rims with calcite.

96-99 cm: Black fresh glass with yellow (2.5Y 7/6) limestone/calcite veins.

SECTION 2

APHYRIC PILLOW BASALT

Aphyric basalt, fine grained gray (7.5YR N5) ranging to pale brown (10YR 6/3) where altered.

Glass rims where shown grade into narrow (<1 cm) black aphanitic and variolitic rims (pale brown - 10YR 6/3) and then to fine grained basalt.

Minor calcite veins where shown.

Vesicles up to 1.5 mm generally round, some irregular concentrate up to ~5% within a few cm of upper pillow margin. Most are empty, a few are clay filled.

SECTION 3

APHYRIC PILLOW BASALT

0-150 cm: Fine grained, aphyric basalt, color gray (2.5Y N5/0) to grayish brown (2.5Y N5/2) in altered parts mainly close to fractures and veins (calcite filled).

28-30, 56-67, and 91-94 cm: Fresh black glass margins, up to 3 cm thick; beginning palagonitization from fracture; variolitic zone is very narrow (a few mm), variolites are <1.5 mm in diameter.

From 0-67 cm: No visible vesicles.

From 68-150 cm: ~2% round vesicles (<1.5 mm in diameter), half empty, half calcite-filled.

SECTION 4

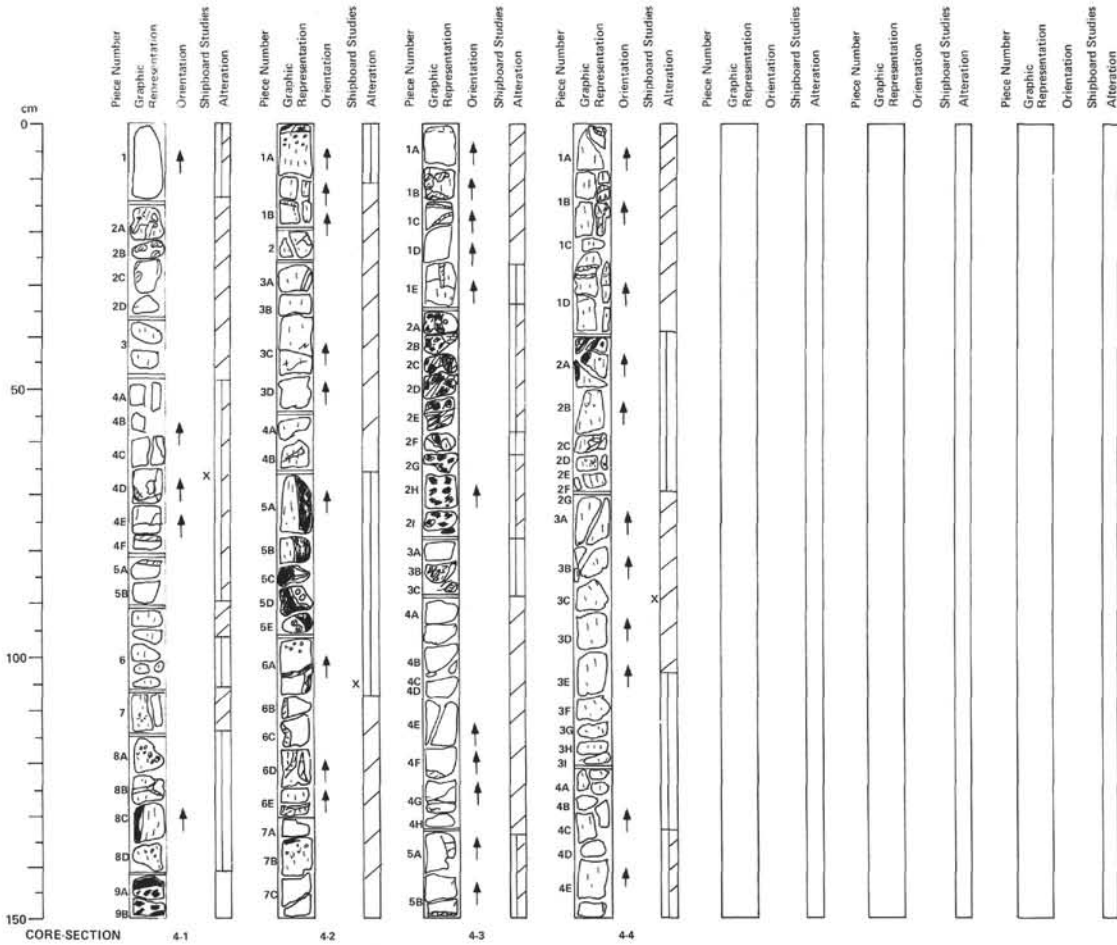
APHYRIC PILLOW BASALT

0-13, 47-50, and 33-39 cm: Fine grained aphyric pillow basalt as in Sections 1-3 - moderately altered. 0-10 cm: 2-7% rounded empty vesicles (1-2 mm) in pillow margin.

40-44 cm: Strongly altered (light brownish gray - 2.5Y 8/2) aphyric basalt as in Sections 1-3. 1-2% rounded empty vesicles (1-3 mm) and 1 rounded calcite-filled vesicle (2 mm).

22-38 cm: Fresh gray (7.5YR N4) aphyric basalt that is slightly to moderately altered. 1-2% tiny (1-2 mm) olivines(?) altered to brown (7.5YR 5/4) clay(?).

16-20 cm: One piece of fresh gray (7.5YR N6) aphyric basalt.



SITE 564, CORE 4

Depth 311.0–320.0 m

SECTION 1

APHYRIC PILLOW BASALT

0–15 and 23–90 m: Fine grained gray (2.5Y N5) aphyric basalt, moderately altered, and coarser grained than previous cores. 5–10% plagioclase needles (1–4 mm) randomly oriented or same in radiating clusters. 1–2% small (1–2 mm) olivines(?) altered to brown (7.5YR 5/4) clay(?). No vesicles and calcite in fractures.
108–139 cm: Fine grained, gray (2.5Y N6) pillow basalt moderately to highly altered to light brownish gray (2.5Y 6/2), finer grained than basalt above. 1–2% round and irregular empty vesicles (1–2 mm) especially in altered pillow rims, <1% irregular calcite-filled vesicles (1–2 mm) calcite in fractures.
128–132 cm: Glass rim.
18–21 cm (Piece 2A): Basalt breccia in calcite matrix.
139–148 cm: Fresh black glass clasts in calcite matrix.

SECTION 2

APHYRIC PILLOW BASALT

0–150 cm: Fine grained, gray (2.5Y N5) aphyric basalt, moderately to more strongly altered to light yellowish brown (2.5Y 6/4) especially near pillow margins and fractures. 1–2% round and irregular vesicles (1–2 mm) empty or filled with calcite especially near pillow margins. Calcite in fractures.
88–94 cm: Black glass pillow chill margins some altered to yellow (10YR 7/8) and strong brown (7.5YR 5/6) clays.

SECTION 3

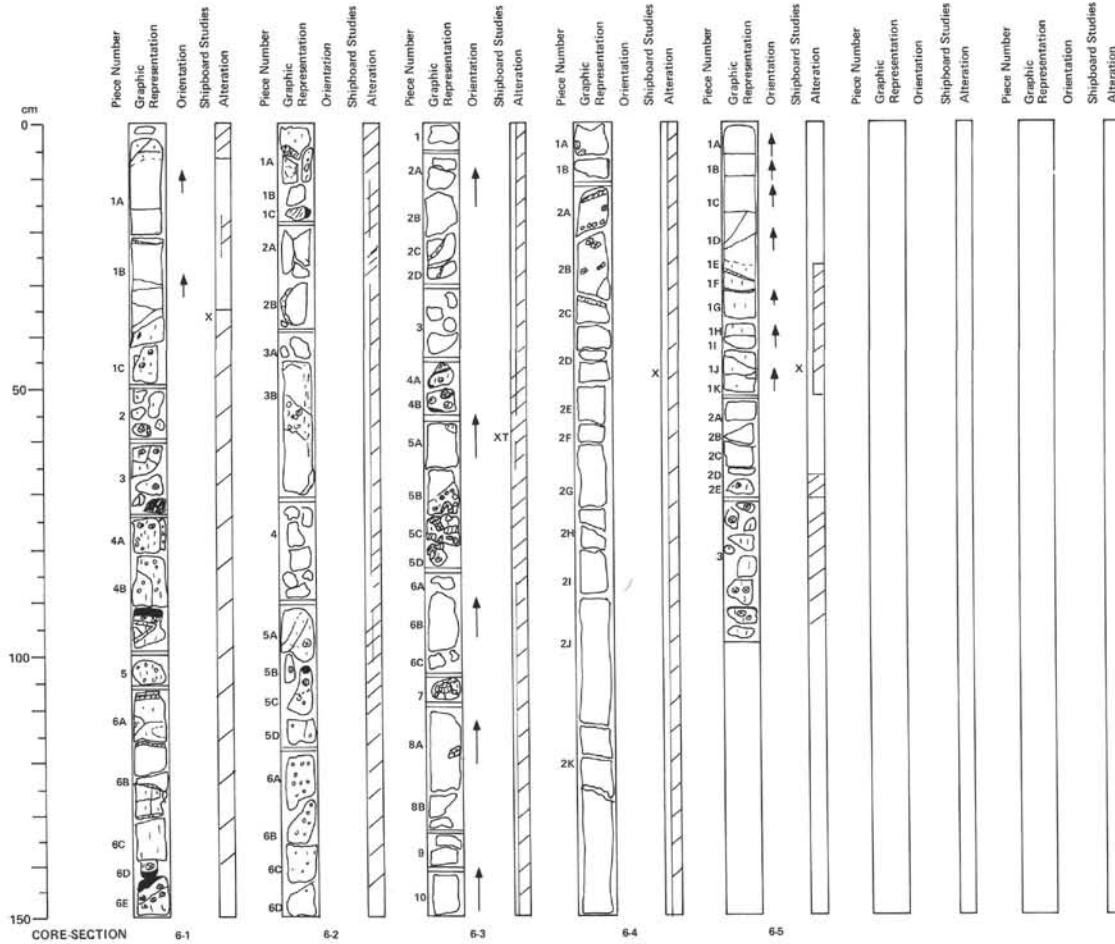
APHYRIC PILLOW BASALT

0–33 cm: Fine grained, gray (7.5YR N5) aphyric basalt. Some moderate alteration to light grayish brown (2.5Y 6/2). 2–3% olivines(?) (1–2 mm) altered to strong brown (7.5YR 5/6) clays(?).
9–13 cm (Piece 1B): ~15% of the basalt consists of large (5–15 mm) irregular calcite-filled interconnecting cavities.
34–77 cm: Black glass clasts (angular to subrounded) in calcite matrix with very pale brown (10YR 6/3) limestone in places.
55–58 cm (Piece 2F): Glass more altered (strong brown – 7.5YR 5/8) and limestone/calcite matrix is yellow (2.5Y 8/6).
78–150 cm (Piece 3B): Finer grained aphyric pillow basalt, moderately altered – <1% visible olivines and vesicles.
82–85 cm: Basalt clast in calcite matrix with pale yellow (2.5Y 8/4) limestone band, more basalt glass in bands.

SECTION 4

APHYRIC PILLOW BASALT

0–150 cm: Fine grained, gray (2.5Y N5) aphyric pillow basalt, moderately to highly altered to light brownish gray (2.5Y 6/2) especially along fractures and pillow margins. <1% rounded, empty vesicles (1–2 mm) mostly in highly altered parts, extensive calcite-filled fracturing.



SITE 564, CORE 6

Depth 329.0–338.0 m

SECTION 1

APHYRIC PILLOW BASALT

0–42 cm: Pillow interior. Aphyric basalt, fine grained dark gray (7.5YR N7). Slightly altered towards brown (10YR 5/1) close to fractures, otherwise fresh. Abundant acicular plagioclase to 3 mm and 2–3% round ~0.5 mm olivine microphenocrysts completely altered brown or dark green.

41–150 cm: Pillow marginal zones. Aphanitic basalt, gray (7.5YR N5) where fresh. Generally altered, light brownish gray to pale brown (10YR 6/2–6/3). Variolitic where shown. Fresh glass where shown, black aphanitic basalt 1–2 cm thick beneath glass then variolitic zone up to several cm thick.

SECTION 2

APHYRIC PILLOW BASALTS

0–30 and 90–115 cm: Pillow margins — aphanitic basalt and glass as in Section 1.

30–90 and 118–150 cm: Fine grained basalt (pillow interior) as in Section 1.

55–82 cm: Irregular, calcite filled vesicles.

115–140 cm: Vesicles, round carbonate filled. Abundance increases downwards from 1–2% to ~8%. Size increases from ~1 mm to 2–3 mm.

SECTION 3

APHYRIC PILLOW BASALT AND MASSIVE FLOW

0–44, 60–70, 88–104, and 112–150 cm: Pillow interior as in Section 1. Probably still part of massive flow begun at 100 cm, Section 2. Altered to a mottled combination of fine grained dark gray (7.5YR N4) towards brown (10YR 5/1). Plagioclase and olivine as in Section 1.

46–59 and 105–109 cm: Highly altered basalt with calcite/limestone blebs. Indications of Mn — calcite — basalt altered light brownish gray to pale brown. Pillow margin? Variolitic as indicated.

70–80 cm: Irregular calcite patches. Sparry calcite intergrown into basalt cavities.

50 cm: New massive flow? Variolitic top.

SECTION 4

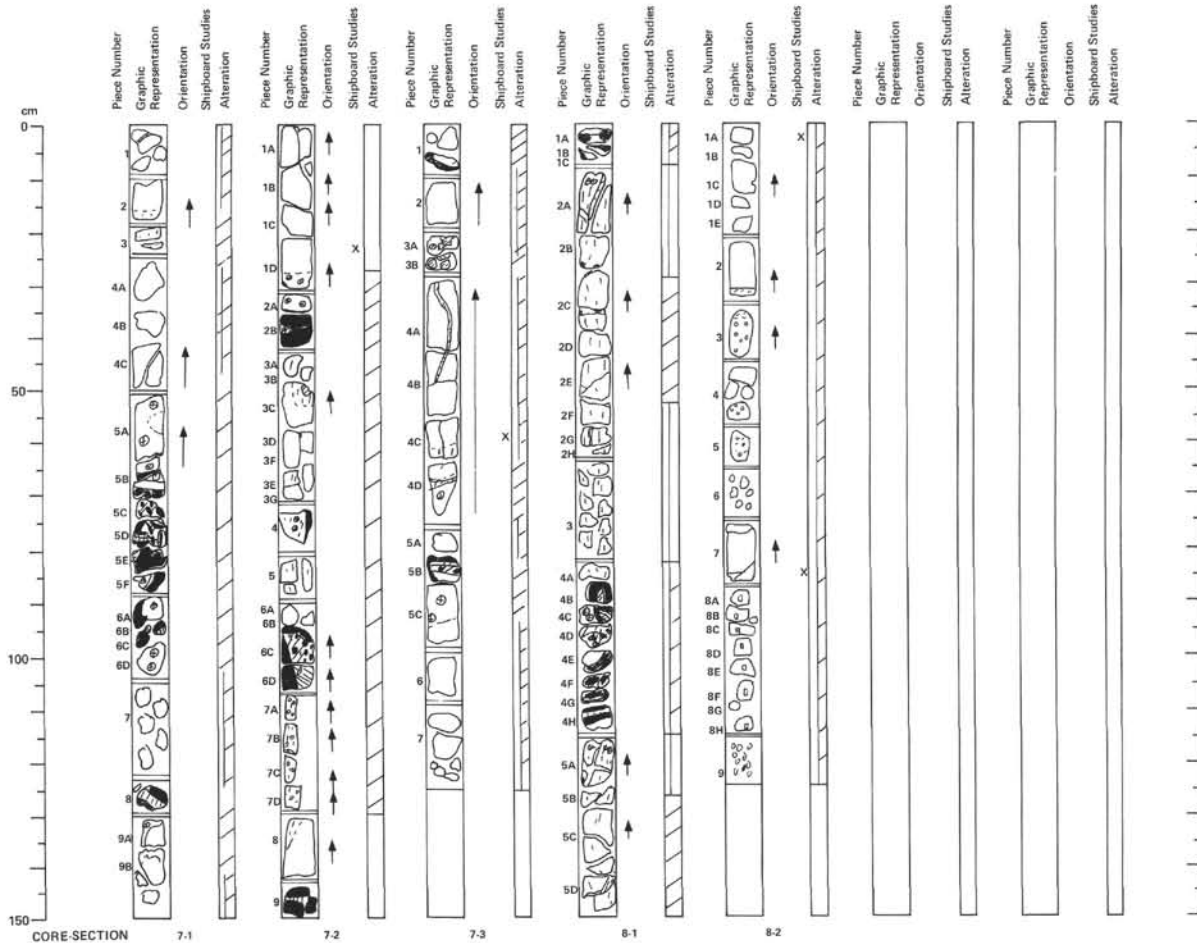
APHYRIC BASALT

0–150 cm:
 Fine grained dark(?) gray (7.5YR N4/0) massive flow interior. Pillow flow continued from Section 3. Calcite patches 1–6 cm as indicated. Large amounts of acicular plagioclase 1–4 mm in length.
 Olivine microphenocrysts present as dark orange brown altered residue anhedral.
 Alteration is moderate. Observed in massive section as mottled gray appearance.

SECTION 5

APHYRIC BASALT

0–64 cm: Fine grained massive basalt flow as in Section 4.
 70–95 cm: Aphanitic and variolitic basalt-pillow margin (base of flow?) material as in Section 1.



SITE 564, CORE 7

Depth 338.0–347.0

SECTION 1

APHYRIC PILLOW BASALT AND GLASS BRECCIA

0–43 and 134–150 cm: Fine grained dark gray (7.5YR N4/0) pillow basalt interior, slightly altered to a mottled gray (7.5YR N5/0), or a light yellowish brown (10YR 6/4).
49–134 cm:

Pillow margin sequence. Interpillow glass grading into variolitic zone (10YR 5/6–10YR 5/8) yellowish brown grading back into gray (7.5YR N 4/0) aphyric basalt. Alteration in variolitic zone to colors described.

Variolitic zone as indicated. Few cm thick aphanitic zone, few cm zone variolitic zone grading into aphyric zone.

Glass as indicated.

63–97 cm: Glass breccia with clasts cemented into a calcite/limestone matrix. Clasts are angular and aligned parallel to each other within a piece. Calcite/limestone may be tinted slight palagonite color, and also a light pink zone is seen.

SECTION 2

APHYRIC PILLOW BASALT

0–28 and 130–140 cm: Fine grained aphyric pillow interior as in Core 6, Section 1, and Core 7, Section 1.
28–128 cm: Aphanitic basalt and glass pillow margin material as in Core 6, Section 1 and Core 7, Section 1.
95–105 cm: Interpillow glass breccia. Matrix part white calcite, part light gray (10YR 7/1) fine grained limestone.

SECTION 3

APHYRIC PILLOW BASALT

0–123 cm: Fine grained dark gray (7.5YR N4/0) pillow basalt interior grading into an interpillow zone, consisting of glass – aphanitic black (10YR N2/0) basalt – variolitic zone. Colors, alteration vesicles, etc. same as Section 1.

SITE 564, CORE 8

Depth 347.0–356.0 m

SECTION 1

APHYRIC PILLOW BASALT

10–84 and 116–150 cm: Fine grained, gray (2.5Y N5) aphyric basalt moderately to highly altered to pale brown (10YR 6/3). Variolitic texture grading through black aphanitic basalt to black glass rims <1% round empty and calcite-filled vesicles (1–2 mm) especially in altered pillow margins. Calcite in fractures.

0–5 and 95–97 cm: Fresh to moderately altered glass clasts (reddish yellow – 7.5YR 6/8 nearest glass to brown – 7.5YR 4/4 further out from glass core) in calcite matrix.

5–8, 86–93, and 99–113 cm: Mostly fresh black glass chill margins with calcite in fractures.

95–97 cm: Sparry calcite rim.

SECTION 2

APHYRIC PILLOW BASALT AND OLIVINE MICRO-PHYRIC BASALT (FLOW?)

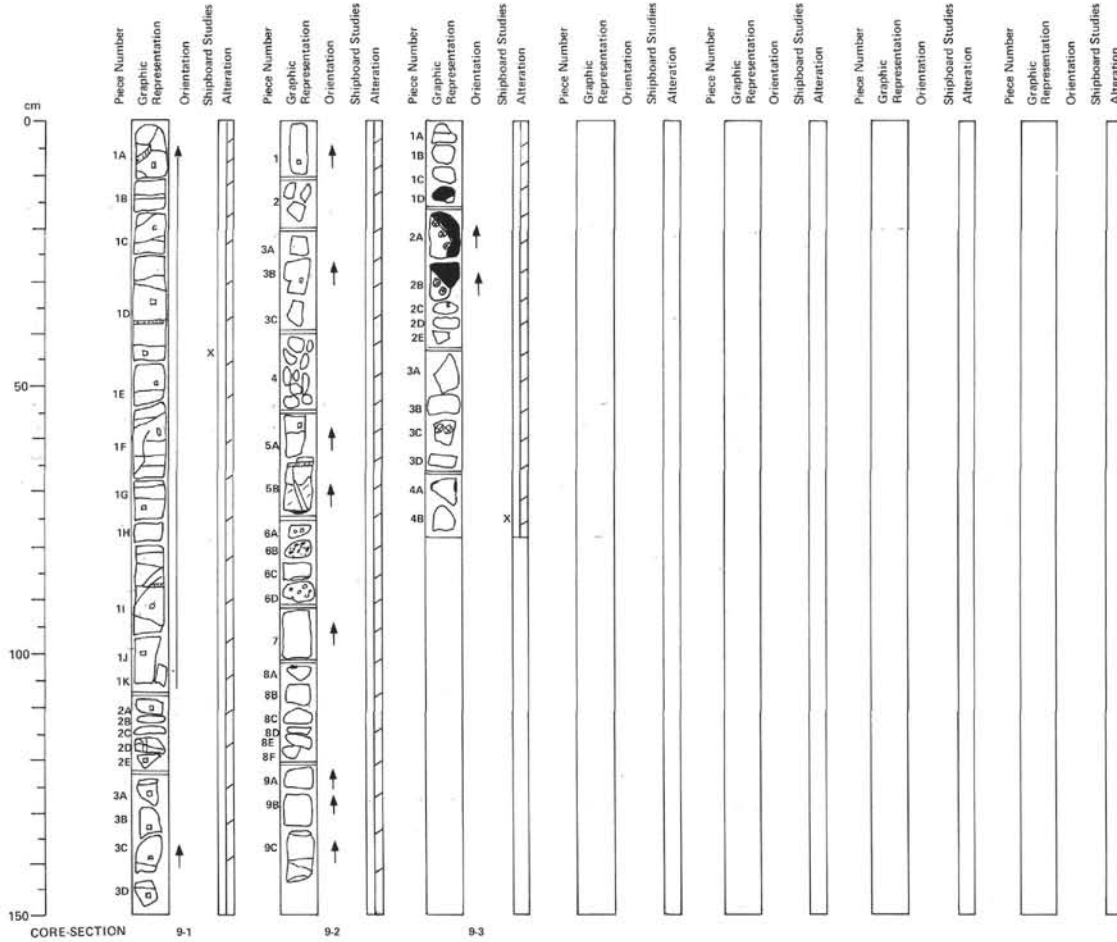
0–65 cm: Aphyric, fine grained basalt, color gray (2.5Y N5/0) to light brownish gray (2.5Y N6/2) in altered parts. Mostly now vesicular, but at:

35–44 and 52–64 cm: Highly vesicular, round, 0.5 to 2 mm in diameter, 5–10%; calcite filled except Piece 5 (empty).

Break at 65 cm.

65–123 cm: Moderately olivine micro-phyric basalt (~5% olivine), fine-grained but coarser than upper pillow basalt. Visible plagioclase laths up to 4 mm. Olivine phenocrysts are randomly scattered, size <1 mm. Replaced by brown and green clay. No visible vesicles.

120 cm: Among the chips occur a few black glass splinters.



SITE 564, CORE 9

Depth 356.0–365.0 m

SECTION 1

MODERATELY TO SPARSELY OLIVINE MICRO-PHYRIC BASALT FLOW

0–150 cm: Fine-grained olivine micro-phyric basalt, color dark gray (5Y 4/1). Olivine phenocrysts are mostly replaced by clay (brown color); size: <1 mm, abundance: <5%. Acicular plagioclase up to 5 mm occurs throughout the section.

1–5 and 128–133 cm: A few scattered lath-shaped or round minerals occur, which look like metallic copper (size: 2 mm to <0.5 mm). Fractures are common and mostly oriented horizontal. They show calcite filling and – in some places – a soft dark to light green mineral on the fracture plane.

SECTION 2

SPARSELY OLIVINE MICRO-PHYRIC TO APHYRIC BASALT FLOW AND APHYRIC BASALT (PILLOW?)

0–75 cm: Sparsely olivine micro-phyric to aphyric basalt, fine-grained, color dark gray (5Y 4/1). Less olivine than in Section 1 (<2%). Plagioclase <1 mm.

73–74 cm: Black glass margin with altered basalt zone about it; color dark grayish brown (10YR 4/2).

Break – end of flow at 75 cm.

76–90 cm: Fragments of:

Pieces A and D: Highly vesicular basalt; round to oval vesicles (<5 mm in diameter) are empty, light green clay filled or coated or calcite filled. Color of basalt: gray (5Y 5/1).

Piece B: Basalt glass breccia. Palagonitized glass clasts <6 mm; calcite cement.

Piece C: Fine grained, sparsely olivine phyric basalt, color dark gray (2.5Y N4/0).

91–143 cm: Fine grained aphyric pillow(?) basalt; color gray (5Y 5/1). No visible vesicles.

SECTION 3

FRAGMENTS OF APHYRIC PILLOW BASALT

0–12 cm: Fine grained, aphyric basalt, color gray (5Y 5/1). Green clay(?) mineral on fracture planes.

13–33 cm: Pieces of chilled pillow margins. Black, highly fractured, calcite-cemented and sometimes palagonitized glass is grading through variolitic zone (varioles <2 mm) into very fine grained, very dark gray (2.5Y N 3/0) aphyric basalt.

34–77 cm: Fine grained aphyric basalt, color gray (5Y 6/1) with visible plagioclase laths (<3 mm). Irregular vesicles are sparsely scattered (<2%) and calcite filled.

56–61 cm: Piece 3C shows varioles <7 mm.

